Targeted Therapy of Tuberculous Meningitis in Rats with Methylprednisolone Composite Nanoparticles

Chuanyang Dai[1#], Xianyue Guan[2#], Guannan Qin[1*]

[1] Department of Emergency, The Affiliated Hospital of Guizhou Medical University, Guiyang, 550004, Guizhou Province, China

[2] Department of Endocrinology, The Second Affiliated Hospital of Guizhou University of Traditional Chinese Medicine, Guiyang, 550003, Guizhou Province, China

[#]These authors contributed equally to this work as co-first author.

ARTICLE INFO

ABSTRACT

It was to investigate the targeted therapeutic effect of methylprednisolone (MPS) composite nanoparticles (NPs) on tuberculous meningitis (TBM) in rats. A total of 180 special pathogen-free (SPF) Sprague Dawley (SD) rats (male) were randomly and equally assigned to the normal control group, TBM infection group, and TBM treatment group. Those in the TBM infection group and the TBM treatment group were injected with Mycobacterium tuberculosis suspension via the tail vein. After the TBM model was established, rats in the TBM treatment group were injected intraperitoneally with methylprednisolone-nano sterically stabilized liposomes (MPS-NSSLs), and those in the normal control group were injected with an equal amount of normal saline. MPS-NSSLs were prepared, and their quality evaluation, encapsulation rate, drug-lipid ratio, and stability were detected. The particle size distribution of MPS-NSSLs was 95.4 ± 0.7 nm, showing a complete spherical structure, and the encapsulation rate was 91.24 ± 0.27 %, and the drug-lipid ratio was about 0.4. After 7 days of treatment, the water content of brain tissue in the TBM infection group was drastically superior to that in the control group ($P<0.05$); Evans blue (EB) content in the TBM infection group was dramatically superior to that in the control group ($P<0.05$). The TBM rat model was successfully established, and this model verified that MPS-NSSLs had the characteristics of high efficiency and low toxicity in the treatment of TBM rats.

Introduction

Tuberculous meningitis (TBM) is a non-suppurative inflammatory disease of the meninges and spinal meninges caused by Mycobacterium tuberculosis. Extrapulmonary tuberculosis involves the nervous system in 5 %-15 % of patients, among which TBM is the most common, accounting for about 70 % of nervous system tuberculosis (1-3). The comprehensive treatment of TBM mainly includes systemic chemotherapy, glucocorticoid therapy, intracranial pressure reduction therapy, local treatment, nutritional support therapy, and brain hernia rescue. In the chemotherapy of TBM, on the one hand, the principles of early, combined, appropriate, regular, and whole-course chemotherapy should be followed. On the other hand, it is necessary to select drugs with bactericidal effects and smooth passage through the blood-brain barrier, and there is a high concentration of drugs in cerebrospinal fluid (4,5). Glucocorticoid treatment for TBM is critical, and the earlier the TBM is used in the acute phase, the better the effect is, and the dose should be sufficient. Methylprednisolone (MPS) is a commonly used drug for the treatment of TBM in the clinic, which can inhibit the activity of lymphocytes, reduce the secretion of inflammatory exudates, and improve neurological disorders (6).

Nanotechnology has been currently adopted in material synthesis, biology, and pharmacy. Nanomaterial particles are extremely small, not easily repelled as foreign bodies in the body, and can be biochemically modified to meet the requirements of drug carriers more easily for biocompatibility in terms of tissue, blood, and immunity (7,8). Liposomes are composed of one or more layers of the lipid bilayer, similar to biofilms in structure, with the characteristics of high encapsulation rate, strong serum stability, strong controllability of drug release, and mature preparation technology, which have become ideal targeted drug carriers and are gradually applied in the research and development of new drugs (9). To further improve the specificity of nano sterically stabilized liposomes (NSSLs) for the treatment site, Naik et al. (2021) (10) linked specific targeting molecules on the lipid surface to bind specific targeting ligands on the surface of tissues and organs, and utilized antigen-antibody specific immune response to achieve targeted drug delivery at therapeutic sites.

MPS (MPS) was used as a therapeutic drug with weak acid and amphiphilic properties. By exploring the establishment of a stable and reliable animal model of TBM in rats, and using the newly developed MPS-nano sterically stabilized liposomes (MPS-NSSLs) as intervention drugs, it was verified that MPS-NSSLs had the unique advantages of high efficiency, low toxicity, and reducing hormone dosage in the treatment of animal TBM, which was of great clinical significance.

Materials and Methods

Materials

180 special pathogen-free (SPF) Sprague Dawley (SD) rats (male, 91.25 ± 10.26 g, Nanjing Junke Biological Co., Ltd.) were fed in separate cages by professionals. All animal experiments were approved by the Affiliated Hospital of Guizhou Medical University Laboratory Animal Center.

Construction of TBM rat model

180 healthy SD rats were randomly and equally rolled into the normal control group, TBM infection group, and TBM treatment group.

The rats in the TBM infection group and treatment group were injected with Mycobacterium tuberculosis suspension via the tail vein, and the normal control group was injected with an equal amount of normal saline. Mycobacterium tuberculosis H37Rv (on 7H9 medium for 2 weeks) of rats in the TBM infection group and TBM treatment group was filtrated, centrifugated, and dispersed, preparing 2.5×10^6 CFU/mL bacterial suspension. 0.2 mL bacterial suspension (bacterial amount 5×10^5 CFU/rat) was injected into the tail vein of each rat, which was placed in a negative pressure environment of (55 ± 15) % humidity and (21 ± 2)℃, maintaining a cycle of 12 h light/12 h dark so that the animals could conveniently obtain food and water. A TBM model was formed after 14 days.

After the formation of a TBM model, the rats in the treatment group were injected with MPS-NSSLs (4 mg/kg·d) intraperitoneally every 24 hours until the rats were sacrificed.

Twenty rats on days 1, 4, and 7 after successful modeling were selected and sacrificed for observation of experimental parameters.

Determination of water content in rat brain tissue

On the 1st, 4th, and 7th day after the model was successfully established, 5 rats of each group were decapitated, the brains were removed as soon as possible, the left cerebral hemisphere was separated, the blood stains on the brain surface were sucked out with filter paper, and the rats were placed into a weighed glass with cover. The wet weight was measured with an electronic analytical balance (graduation value 0.1 mg), and the rats were placed into a 110℃ constant temperature drying oven for 24-36 hours to a constant weight (the difference between the two weighing samples was ≤ 0.2 mg). After dry weight was measured, the percentage of brain water content (%) was calculated with the Elliot equation.

$$Brain\ water\ content\ (\%) = (wet\ weight - dry\ weight)/wet\ weight \times 100\% \quad [1]$$

Evans blue (EB) assay

On the 1st, 4th, and 7th day after successful modeling, 5 rats of each group were injected with 2 % EB (2 mg/kg) through the tail vein 1 hour before sacrifice and anesthetized by intraperitoneal injection of 1 % pentobarbital sodium, and the heart was rapidly disclosed to expose and perfused with 500 mL of normal saline at 37℃. resulting in clear fluid from the right atrial appendage. EB content in brain tissue was measured by the formamide digestion method: brain tissue samples were extracted from the cortex of the injured side, and after measurement of wet weight, they were placed into a centrifuge tube containing formamide of 4 times the volume of brain tissue samples. After covering, a water bath was carried out at 5℃ for 24 hours. They were centrifuged at 1,500 r/min for 10 min, the supernatant was taken, the absorbance (A) value was measured at the EB maximum absorption spectrum of 635 nm, and the EB content was obtained by plotting the standard curve.

Determination of gene and protein expression

On the 1st, 4th, and 7th day after successful modeling, 10 rats of each group, the gene level of vascular endothelial growth factor (VEGF) and receptor in the brain tissue of the TBM infection group was detected by RT-PCR; the protein level of VEGF and receptor in the brain tissue of the TBMinfection group was detected by Western blot; the protein level of VEGF and receptor in the brain tissue of the TBMinfection group was detected by pathological staining.

Preparation of MPS-NSSLs

MPS-NSSLs were prepared by film dispersion method, with the preparation process illustrated in Figure 1.

(i) Distearoylphosphatidylcholine (DSPC), cholesterol, distearoylphosphatidylethanolamine-polyethylene glycol (DSPE-PEG2000), and distearoylphosphatidylethanolamine-polyethylene glycol-carboxyl (DSPE-PEG2000-COOH) (molar ratio 20: 14.5: 1.8: 0.05) were weighed, dissolved in a round-bottom glass test tube containing trichloromethane/methanol mixture (volume ratio of 2:1). It was blown dry by nitrogen to form an adherent and uniform film. The organic solvent was removed by vacuum drying overnight at room temperature.

(ii) An appropriate amount of 200 mM calcium acetate solution was hydrated, and the liposomes were dispersed by ultrasound bath (30 min, 250 w) at 72℃.

(iii) Liposome suspension was obtained by successively passing the light blue opalescent solution after ultrasound through filter membranes of 0.4 μm, 0.2 μm, and 0.1 μm using a lipid extruder (Avanti® Mini-Extruder, Avanti Polar Lipids, USA) and pushing 13-17 times at each layer.

(iv) Liposome suspension was dialysed overnight at 4℃ in 0.9 % normal saline with a dialysis tube (molecular weight 300kDa) and stored at 4℃.

(v) The prescription amount of MPS was weighed and dissolved in 0.9 % normal saline to prepare 4.2 mM MPS solution, which was mixed with the prepared liposome suspension, heated in water bath at 70℃ for 40 min, and stored at 4℃.

(vi) The unencapsulated free MPS was removed by a gel filtration column (Superose G-25) and stored at 4℃.

Isolation and purification of MPS-NSSLs

Dextran G25 (10×150 mm) column was pre-equilibrated by eluent (0.001 M Na_2HPO_4, 0, 15 M NaCl, pH 7.4) and connected to a Bio Logic LP low-pressure chromatography (Bio-rad, USA). 0.5 mL of drug-loaded liposomes were injected into the preloaded column at a flow rate of 1 mL/min, UV absorption values were detected at 280 nm, and liposomes and unencapsulated drugs were collected according to the order of peak appearance.

Quality evaluation of MPS-NSSLs

The liposomes were diluted with ultrapure water and added to the sample cell, and measurements were perfor-
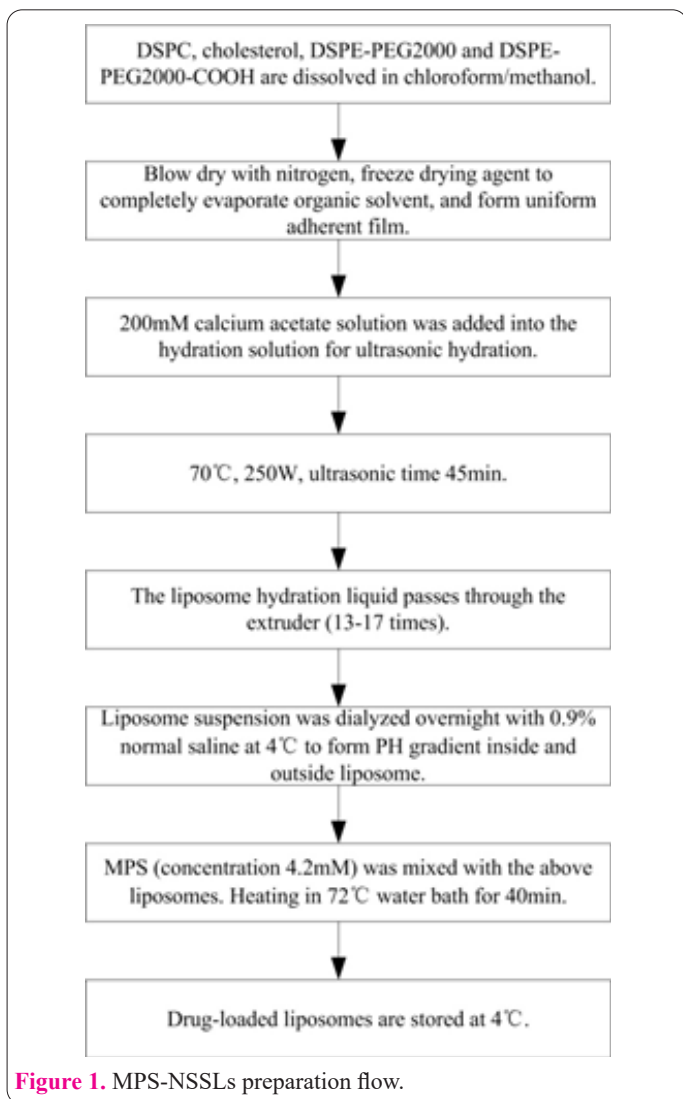
Figure 1. MPS-NSSLs preparation flow.

med on a ZS90 Laser Particle Size Analyzer (Malvern, UK) with three replicates for each sample. 5 μL of MPS-NSSLs was dropped onto the copper mesh, and the excess was absorbed by the filter paper. On a homemade rapid freezing device, the copper mesh was rapidly projected into liquid nitrogen ethane that was fully cooled by liquid nitrogen, the copper mesh was kept submerged in liquid nitrogen, transferred to a sample transfer rack, and observed using a tecnai G2 F20 field emission transmission electron microscope (FEI, Netherlands) at -176°C with an acceleration voltage of 200 kV. Images were recorded using an FEI Eagle4k × 4k CCD and observed using a low-dose technique with an electron dose ≤ 10 e/Å2.

Detection of encapsulation rate, drug-lipid ratio, and stability of MPS-NSSLs

0.5 mL MPS-NSSLs were taken and the unencapsulated free MPS was separated by Superose G-25 (10 × 150 mm) with pre-equilibrated eluent (0.001 M Na_2HPO_4, 0, 15 M NaCl, pH 7.4) as a free drug (W_{free}). In addition, 0.5 mL MPS-NSSLs and 5 mL methanol were used as the total drug dose (W_{total}). Free drug (W_{free}) and total drug dose (W_{total}) were determined by high-performance liquid chromatography (HPLC). The encapsulation rate was calculated as follows.

$$Medicine-fat\ ratio = W_{MPS}\ /\ W_{lipids} \times 100\% \qquad [2]$$

The calculation of the measured actual encapsulation

amount (W_{MPS}) of liposomes, phospholipid amount (W_{lipids}) of known drug-loaded liposomes, and the drug-lipid ratio were as follows.

$$Medicine-fat\ ratio = W_{MPS}\ /\ W_{lipids} \times 100\% \qquad [3]$$

An appropriate amount of MPS-NSSLs was taken, evenly divided into 3 parts, and placed at 4°C. Samples were taken at 0, 4, 8, and 12 weeks to obtain the encapsulation rate, determining the stability of MPS-NSSLs.

Statistical methods

Excel 2016 was employed for the collation of all data, and SPSS 19.0 for the statistical analysis of treatment effect indicators. The measurement data in line with normal distribution were denoted as mean ± standard deviation ($\bar{x}$±s), and the count data percentage (%). The comparison was carried out by one-way analysis of variance (ANOVA). $P < 0.05$ indicated the difference was considerable.

Results

Isolation and purification of MPS-NSSLs

Due to the different molecular weights, the UV absorption curves of MPS-NSSLs and MPS purified by Bio Logic LP low-pressure chromatography and Superose G-25 (10 × 150 mm) were inconsistent. The MPS-NSSLs with large molecular weight were eluted first, and the MPS-NSSLs peak appeared, and then the free MPS peak appeared. The separation effect of MPS-NSSLs and MPS was good (Figure 2).

Particle size distribution

The particle size distribution of MPS-NSSLs was 95.4 ± 0.7 nm, which showed a positive distribution with uniform distribution and a small span (Figure 3).

Morphological observation

MPS-NSSLs were observed under a field emission transmission electron microscope, and it showed a complete spherical structure with uniform distribution (Figure 4).

Encapsulation rate, drug-to-lipid ratio, and stability

The encapsulation rate of MPS-NSSLs to MPS reached 91.24 ± 0.27 %, with a drug-to-lipid ratio of about 0.4; MPS-NSSLs could be stably placed at 4°C for not less than 12 weeks, and the encapsulation rate of MPS-NSSLs
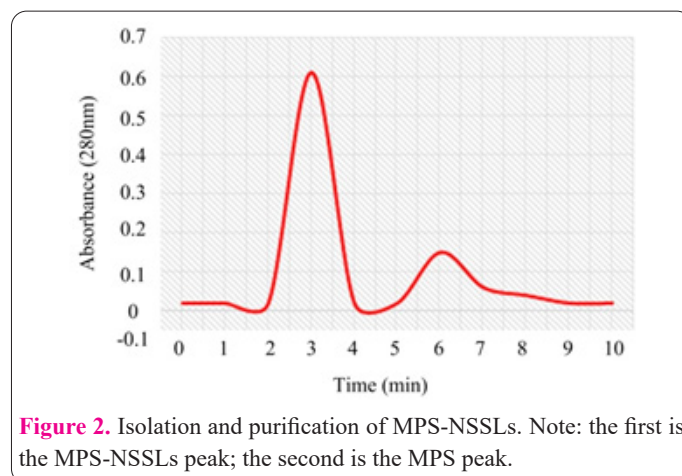

Figure 2. Isolation and purification of MPS-NSSLs. Note: the first is the MPS-NSSLs peak; the second is the MPS peak.
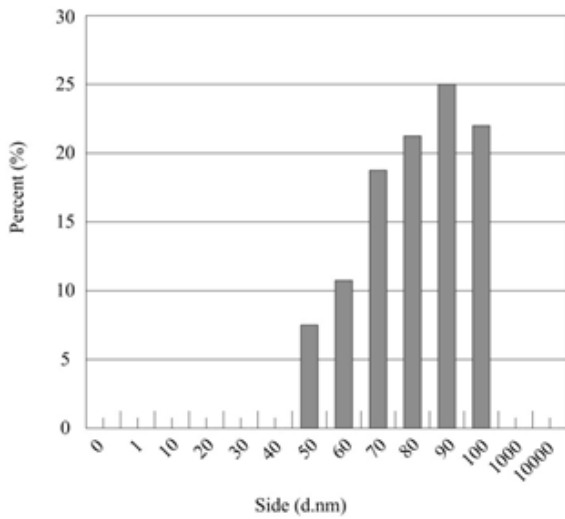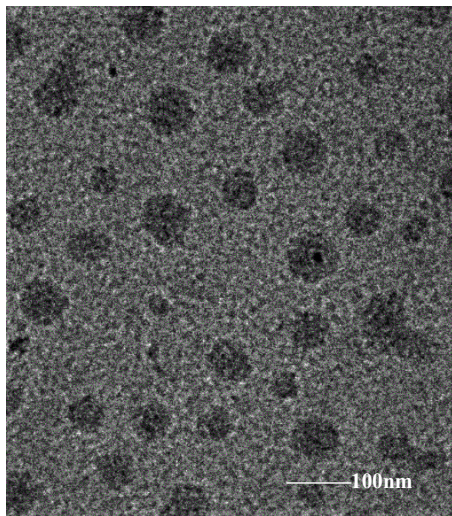
Figure 3. Particle size distribution of MPS-NSSLs.

Figure 4. Morphological observation of MPS-NSSLs.

to the drug tended to decrease, but it was not significant (Figure 5).

VEGF and receptor mRNA in brain tissue

After 4 days of treatment, the relative expression of VEGF and receptor mRNA in brain tissue of the TBM infection group was markedly higher versus the control group ($P < 0.05$). VEGF and receptor mRNA in brain tissue of the TBM treatment group was significantly lower than that of the TBM infection group ($P < 0.05$). After 7 days of treatment, VEGF and receptor mRNA in brain tissue of the TBM infection group was substantially superior to the control group ($P < 0.05$). VEGF and receptor mRNA in the brain tissue of the TBM treatment group was remarkably inferior to that of the TBM infection group ($P < 0.05$) (Figure 6).

Pathological observation of VEGF and receptor in brain tissue

The infection group had diffuse congestion, edema, inflammatory exudation, and many tuberculosis nodules versus the control group. After targeted therapy with MPS-NSSLs, inflammation was significantly reduced (Figure 7).

Determination of brain tissue water content

4 days after the intervention, the brain tissue water

content of the TBM infection group was drastically higher versus the control group ($P < 0.05$); the brain tissue water content of the treatment group was superior to the control group ($P < 0.05$). Seven days after the intervention, the brain tissue water content of the TBM infection group was superior to the control group ($P < 0.05$); the brain tissue water content of the treatment group differed not greatly from that of the control group ($P > 0.05$) (Figure 8). It demonstrated the alleviating effect of MPS-NSSLs on TBM.

Determination of EB content

After 4 days of intervention, the content of EB in the TBM infection group was superior to the control group ($P < 0.05$); the content of EB in the brain tissue of the treatment group was higher than the control group ($P < 0.05$). After 7 days of intervention, the content of EB in the TBM infection group was higher versus the control group ($P < 0.05$); EB content differed not notably between the treat-
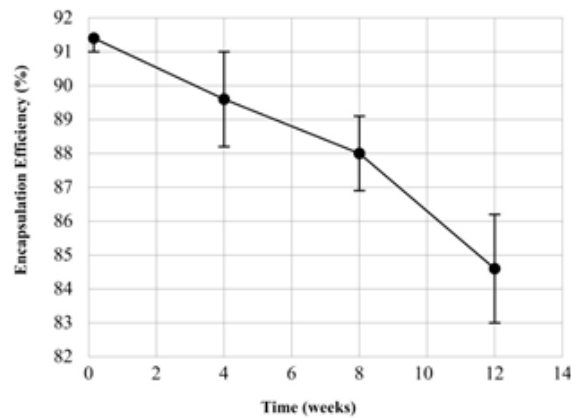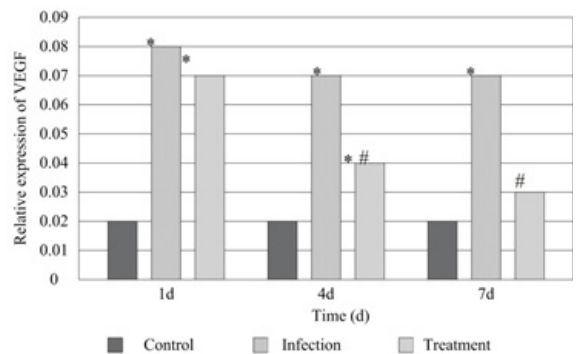

Figure 5. Determination of encapsulation rate of MPS-NSSLs.

Figure 6. Expression of VEGF and receptor mRNA in brain tissue. Note: * and # indicate statistically significant differences between the control group and infection group, respectively ($P < 0.05$).
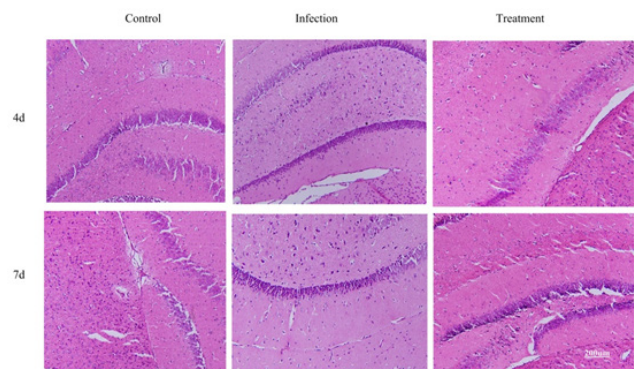

Figure 7. Determination of encapsulation rate of MPS-NSSLs. HE staining after targeted therapy with MPS-NSSLs.
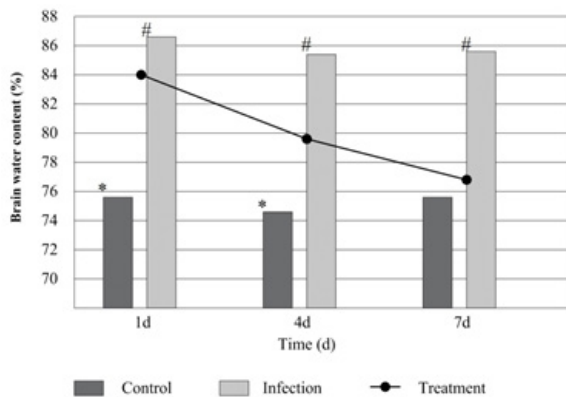
Figure 8. Comparison of brain tissue water content. Note: * and # meant there was statistical significance compared with the treatment group and control group ($P < 0.05$).
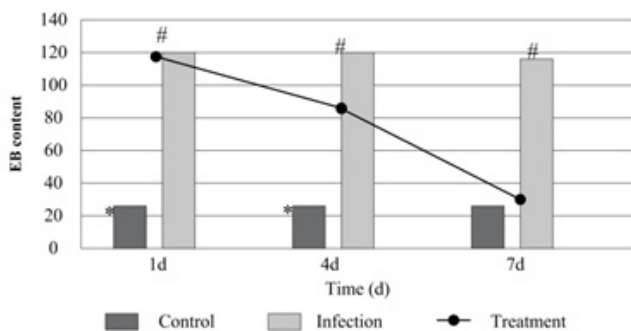

Figure 9. Comparison of EB content. Note: * and # indicated a considerable difference compared between the treatment group and the control group ($P < 0.05$).

ment group and the control group ($P > 0.05$) (Figure 9).

Discussion

Most TBM originates from hematogenous spread, and its lesions are severe and involved in a wide range. The main pathological changes of the disease are extensive tuberculous exudation of the meninges and ependyma at the base of the brain. In addition, tuberculous endarteritis or tuberculous panarteritis occurs in the cerebral arteries, causing thrombosis, which leads to cerebral infarction and encephalomalacia. Meningeal lesions at the base of the brain can lead to dysfunction of the optic nerve, oculomotor nerve, abducens nerve, as well as facial nerve in severe cases (11-15). Meninges on the cerebrospinal fluid circulation pathway, due to exudation causing thickening, adhesions, causing stenosis and obstruction of the pathway, develop communicating or obstructive hydrocephalus (16-18). Therefore, controlling tuberculous exudation and reducing intracranial pressure is the key to the treatment of the disease. MPS has the advantages of strong effect and rapid onset and is suitable for the treatment of TBM. MPS diffuses through the cell membrane and binds to specific receptors in the cytoplasm. The resulting conjugates enter the nucleus and bind to DNA to initiate the transcription of mRNAs, followed by the production of various enzyme proteins, which exert their strong anti-allergic effects and inhibit the migration and activation of inflammatory cells and the release of inflammatory mediators (19). Beardsley et al. (2019) (20) explored the use of MPS in the treatment of viral meningitis, which can not only reduce the inflammatory response and protect the blood-brain barrier, but

also reduce intracranial pressure, reduce neuron-specific enolase content, facilitate the recovery of brain injury, and avoid or reduce the occurrence of neurological sequelae, which is similar to the results of this experiment.

In the 1970s, biologically targeted drug delivery was rapidly developed in the medical field, providing new ideas for meningitis-specific targeted drug delivery (21-23). With more and more studies on targeted drug delivery systems with high efficiency and low toxicity by scholars, nanotechnology has shown a wide application prospect in the field of medicine and pharmaceuticals. Nanomedicines refer to drugs made by nanoscale polymer nanoparticles (NPs), nanospheres (NS), and nano-capsules (NC) as targeting carriers to combine with drugs (24-26). Since the drug acts on the human body, the carrier material is required to be non-toxic, biocompatible, and biodegradable. Liposomes are composed of one or more layers of lipid bilayers, containing water-like vesicles, which are similar to biofilms in structure, are non-toxic, have good biocompatibility, and can encapsulate a variety of substances in their aqueous phase and membranes, become the most ideal choice of targeted drug carriers. In order to reduce the immune side effects caused by heterologous antibodies in the human body, MPS-NSSLs were added with the coupling agent DSPE-PEG2000-COOH on their surface and their various properties were evaluated. The particle size distribution of MPS-NSSLs was 95.4 ± 0.7 nm, the encapsulation rate of MPS reached 91.24 ± 0.27 %, and the drug-to-lipid ratio was about 0.4. The rat model experiments confirmed that MPS-NSSLs had specific targeting and good stability, which was consistent with the results of Weng et al. (2021) (27). There are other reports (28-31) in this regard.

In summary, this experiment successfully established a rat model of TBM and verified that MPS-NSSLs were highly effective and low toxic for the treatment of TBM in rats through this model. It provides a research idea and theoretical basis for exploring the targeted therapy of TBM, and can further optimize the targeted drugs in the future, including the following two aspects: to explore new brain-specific targeted molecules, try to connect double antibody molecules on the liposome surface, and further improve the tissue targeting of drugs; to explore the coating methods of different therapeutic drugs and expand the application range of brain tissue-targeted nanoliposome drugs.

Conclusion

180 SD rats were rolled into the control group, and TBM infection group, and the TBM treatment group. It was applied in the treatment of a rat model of TBM by prepared MPS-NSSLs. In this experiment, a rat model of TBM was successfully established, and this model verified that MPS-NSSLs were highly effective and low toxic for the treatment of TBM in rats. The limitation is that the coating method of the drug is single, and the optimal coating method of brain tissue-targeted nanoliposome drugs needs to be explored at a later stage. In conclusion, an MPS-NSSL is constructed, and it has promising clinical applications.

Funding

2881).

References

1. Davis AG, Rohlwink UK, Proust A, Figaji AA, Wilkinson RJ. The pathogenesis of tuberculous meningitis. J Leukoc Biol. 2019 Feb;105(2):267-280. doi: 10.1002/JLB.MR0318-102R. Epub 2019 Jan 15. PMID: 30645042; PMCID: PMC6355360.

2. Wilkinson RJ, Rohlwink U, Misra UK, van Crevel R, Mai NTH, Dooley KE, Caws M, Figaji A, Savic R, Solomons R, Thwaites GE; Tuberculous Meningitis International Research Consortium. Tuberculous meningitis. Nat Rev Neurol. 2017 Oct; 13(10):581-598. doi: 10.1038/nrneurol.2017.120. Epub 2017 Sep 8. PMID: 28884751.

3. Donovan J, Figaji A, Imran D, Phu NH, Rohlwink U, Thwaites GE. The neurocritical care of tuberculous meningitis. Lancet Neurol. 2019 Aug; 18(8):771-783. doi: 10.1016/S1474-4422(19)30154-1. Epub 2019 May 17. PMID: 31109897.

4. Méchaï F, Bouchaud O. Tuberculous meningitis: Challenges in diagnosis and management. Rev Neurol (Paris). 2019 Sep-Oct;175(7-8):451-457. doi: 10.1016/j.neurol.2019.07.007. Epub 2019 Aug 2. PMID: 31383464.

5. Daniel BD, Grace GA, Natrajan M. Tuberculous meningitis in children: Clinical management & outcome. Indian J Med Res. 2019 Aug;150(2):117-130. doi: 10.4103/ijmr.IJMR_786_17. PMID: 31670267; PMCID: PMC6829784.

6. Schlatter J, Nguyen D, Zamy M, Kabiche S, Fontan JE, Cisternino S. Safety of intrathecal route: focus to methylprednisolone acetate (Depo-Medrol) use. Eur Spine J. 2019 Jan;28(1):21-30. doi: 10.1007/s00586-017-5387-x. Epub 2017 Nov 18. PMID: 29151132.

7. Hassan S, Hassan FU, Rehman MS. Nano-particles of Trace Minerals in Poultry Nutrition: Potential Applications and Future Prospects. Biol Trace Elem Res. 2020 Jun;195(2):591-612. doi: 10.1007/s12011-019-01862-9. Epub 2019 Aug 31. PMID: 31473896.

8. Manigrasso M, Protano C, Vitali M, Avino P. Where Do Ultrafine Particles and Nano-Sized Particles Come From? J Alzheimers Dis. 2019;68(4):1371-1390. doi: 10.3233/JAD-181266. PMID: 31006689.

9. Zhang Q, Wu W, Zhang J, Xia X. Antimicrobial lipids in nano-carriers for antibacterial delivery. J Drug Target. 2020 Mar;28(3):271-281. doi: 10.1080/1061186X.2019.1681434. Epub 2019 Oct 24. PMID: 31613147.

10. Naik H, Sonju JJ, Singh S, Chatzistamou I, Shrestha L, Gauthier T, Jois S. Lipidated Peptidomimetic Ligand-Functionalized HER2 Targeted Liposome as Nano-Carrier Designed for Doxorubicin Delivery in Cancer Therapy. Pharmaceuticals (Basel). 2021 Mar 6;14(3):221. doi: 10.3390/ph14030221. PMID: 33800723; PMCID: PMC8002094.

11. Stavrou M, Yeo JM, Slater AD, Koch O, Irani S, Foley P. Case report: meningitis as a presenting feature of anti-NMDA receptor encephalitis. BMC Infect Dis. 2020 Jan 7;20(1):21. doi: 10.1186/s12879-020-4761-1. PMID: 31910823; PMCID: PMC6947964.

12. Kang HS, Kim JE, Yoo JR, Oh H, Kim M, Kim YR, Heo ST. Aseptic Meningitis Following Second Dose of an mRNA Coronavirus Disease 2019 Vaccine in a Healthy Male: Case Report and Literature Review. Infect Chemother. 2022 Jan 27. doi: 10.3947/ic.2021.0131. Epub ahead of print. PMID: 35132836.

13. Yang X, Zhang C, Zhang J, Chen G, Zhao L, Yang P, Li H, Long Y. Autoimmune glial fibrillary acidic protein astrocytopathy mimics infectious meningitis: Two case reports. Mult Scler Relat Disord. 2020 Oct;45:102350. doi: 10.1016/j.msard.2020.102350. Epub 2020 Jul 1. PMID: 32645637.

14. Manyelo CM, Solomons RS, Walzl G, Chegou NN. Tuberculous Meningitis: Pathogenesis, Immune Responses, Diagnostic Challenges, and the Potential of Biomarker-Based Approaches. J Clin Microbiol. 2021 Feb 18;59(3):e01771-20. doi: 10.1128/JCM.01771-20. PMID: 33087432; PMCID: PMC8106718.

15. Dian S, Hermawan R, van Laarhoven A, Immaculata S, Achmad TH, Ruslami R, Anwary F, Soetikno RD, Ganiem AR, van Crevel R. Brain MRI findings in relation to clinical characteristics and outcome of tuberculous meningitis. PLoS One. 2020 Nov 13;15(11):e0241974. doi: 10.1371/journal.pone.0241974. PMID: 33186351; PMCID: PMC7665695.

16. Soria J, Chiappe A, Gallardo J, Zunt JR, Lescano AG. Tuberculous Meningitis: Impact of Timing of Treatment Initiation on Mortality. Open Forum Infect Dis. 2021 Jun 30;8(7):ofab345. doi: 10.1093/ofid/ofab345. PMID: 34307735; PMCID: PMC8297700.

17. Garg RK, Rizvi I, Malhotra HS, Uniyal R, Kumar N. Management of complex tuberculosis cases: a focus on drug-resistant tuberculous meningitis. Expert Rev Anti Infect Ther. 2018 Nov;16(11):813-831. doi: 10.1080/14787210.2018.1540930. PMID: 30359140.

18. Hong SI, Kim T, Jung J, Park SY, Chong YP, Lee SO, Choi SH, Kim YS, Woo JH, Lee SA, Kim SH. Tuberculous Meningitis-Mimicking Varicella-Zoster Meningitis. Infect Chemother. 2017 Jun;49(2):123-129. doi: 10.3947/ic.2017.49.2.123. PMID: 28681577; PMCID: PMC5500267.

19. Kubre J, Goyal V, Saigal S, Sharma JP, Joshi R. Tuberculous Meningitis Presenting as Cerebral Salt Wasting Syndrome: A Review of Literature with Clinical Approach to Hyponatremia. Neurol India. 2021 Jan-Feb;69(1):190-193. doi: 10.4103/0028-3886.310074. PMID: 33642300.

20. Beardsley J, Hoang NLT, Kibengo FM, Tung NLN, Binh TQ, Hung LQ, Chierakul W, Thwaites GE, Chau NVV, Nguyen TTT, Geskus RB, Day JN. Do Intracerebral Cytokine Responses Explain the Harmful Effects of Dexamethasone in Human Immunodeficiency Virus-associated Cryptococcal Meningitis? Clin Infect Dis. 2019 Apr 24;68(9):1494-1501. doi: 10.1093/cid/ciy725. PMID: 30169607; PMCID: PMC6481995.

21. Chaurasia PK, Bharati SL, Yadava S. Nano-reduction of gold and silver ions: A perspective on the fate of microbial laccases as potential biocatalysts in the synthesis of metals (gold and silver) nano-particles. Curr Res Microb Sci. 2021 Dec 14;3:100098. doi: 10.1016/j.crmicr.2021.100098. PMID: 35024642; PMCID: PMC8732750.

22. Chen Y, Zhang X, Liu W. Effect of metal and metal oxide engineered nano particles on nitrogen bio-conversion and its mechanism: A review. Chemosphere. 2022 Jan;287(Pt 1):132097. doi: 10.1016/j.chemosphere.2021.132097. Epub 2021 Sep 1. PMID: 34523458.

23. Atmakuri A, Palevicius A, Vilkauskas A, Janusas G. Review of Hybrid Fiber Based Composites with Nano Particles-Material Properties and Applications. Polymers (Basel). 2020 Sep 14;12(9):2088. doi: 10.3390/polym12092088. PMID: 32937898; PMCID: PMC7570160.

24. Kawanishi M, Yoneda R, Totsuka Y, Yagi T. Genotoxicity of micro- and nano-particles of kaolin in human primary dermal keratinocytes and fibroblasts. Genes Environ. 2020 Apr 16;42:16. doi: 10.1186/s41021-020-00155-1. PMID: 32322315; PMCID: PMC7164293.

25. Karpenko AA, Odintsov VS, Istomina AA. Micro-nano-sized polytetrafluoroethylene (teflon) particles as a model of plastic pollution detection in living organisms. Environ Sci Pollut Res Int. 2022 Feb;29(8):11281-11290. doi: 10.1007/s11356-021-16487-6. Epub 2021 Sep 17. PMID: 34532808.

26. Xu L, Guo Z, Jiang H, Xu S, Ma J, Hu M, Yu J, Zhao F, Huang

T. Dimethylglyoxime Clathrate as Ligand Derived Nitrogen-Doped Carbon-Supported Nano-Metal Particles as Catalysts for Oxygen Reduction Reaction. Nanomaterials (Basel). 2021 May 18;11(5):1329. doi: 10.3390/nano11051329. PMID: 34070015; PMCID: PMC8157886.

27. Weng D, Yin ZF, Chen SS, He X, Li N, Chen T, Qiu H, Zhao MM, Wu Q, Zhou NY, Lu LQ, Tang DL, Song JC, Li HP. Development and assessment of the efficacy and safety of human lung-targeting liposomal methylprednisolone crosslinked with nanobody. Drug Deliv. 2021 Dec;28(1):1419-1431. doi: 10.1080/10717544.2021.1921073. PMID: 34223777; PMCID: PMC8259875.

28. Alavi M, Hamblin M. Antibacterial silver nanoparticles: effects on bacterial nucleic acids. Cell Mol Biomed Rep 2023; 3(1): 35-40. doi: 10.55705/cmbr.2022.361677.1065.

29. Alavi M, Hamblin M, Mozafari, M. Rose Alencar de Menezes, I., Douglas Melo Coutinho, H. Surface modification of SiO2 nanoparticles for bacterial decontaminations of blood products. Cell Mol Biomed Rep 2022; 2(2): 87-97. doi: 10.55705/cmbr.2022.338888.1039.

30. Alavi M, Rai M, Martinez F, Kahrizi D, Khan H. Rose Alencar de Menezes, I., Douglas Melo Coutinho, H., Costa, J. The efficiency of metal, metal oxide, and metalloid nanoparticles against cancer cells and bacterial pathogens: different mechanisms of action. Cell Mol Biomed Rep 2022; 2(1): 10-21. doi: 10.55705/cmbr.2022.147090.1023.

31. Alavi M, Rai M. Antisense RNA, the modified CRISPR-Cas9, and metal/metal oxide nanoparticles to inactivate pathogenic bacteria. Cell Mol Biomed Rep 2021; 1(2): 52-59. doi: 10.55705/cmbr.2021.142436.1014.